PAPER

Check for updates

A highly conductive quasi-solid-state electrolyte based on helical silica nanofibers for lithium batteries†

Jiemei Hu,[a] Haoran Wang,[a] Yonggang Yang, [iD][a] Yi Li [iD]*[a] and Qi-hui Wu [iD]*[b]

The replacement of flammable liquid electrolytes by inorganic solid ones is considered the most effective approach to enhancing the safety of Li batteries. However, solid electrolytes usually suffer from low ionic conductivity and poor rate capability. Here we report a unique quasi-solid-state electrolyte based on an inorganic matrix composed of helical tubular silica nanofibers (HSNFs) derived from the self-assembly of chiral low-molecular-weight amphiphiles. The HSNFs/ionic liquid quasi-solid-state electrolyte has high thermal stability (up to ~370 °C) and good ionic conductivity (~3.0 mS cm^{-1} at room temperature). When tested as the electrolyte in a LiFePO$_4$/Li cell, excellent rate capability and good cycling stability are demonstrated, suggesting that it has potential be the electrolyte for a new generation of safer Li batteries.

1. Introduction

Rechargeable Li batteries (LBs) are currently the most attractive electrochemical energy storage devices due to their high energy and power densities and long cycling life.[1,2] Advances in both energy density and safety are considered a critical step for portable electronic devices and electric (or hybrid electric) vehicles.[3-5] To date, considerable efforts have been devoted to the use of Li metal anodes to replace the commonly used carbon anodes[6] because the theoretical capacity of Li (3860 mA h g^{-1}) is about one order of magnitude greater than that of the graphitic anodes (372 mA h g^{-1}). Moreover, the use of Li metal anodes would increase the cell voltage, further increasing the energy density of the battery.[7-9] However, the practical applications of Li metal anodes in commercial cells are limited by two notorious safety concerns: the formation and proliferation of Li dendrites during charging[10-15] and the flammability and leakage of the conventional organic electrolytes.[16] In particular, lithium dendrites may accelerate detrimental reactions with the electrolyte and even render catastrophic cell failure by internal short circuiting when Li dendrites reach the cathode.[12,17]

Several strategies have been proposed to suppress the growth of Li dendrites. One interesting approach is the *in situ* growth of a predetermined solid electrolyte interface (SEI) on Li anode by introducing additives,[18,19] highly concentrated[20,21] and special Li salts[22] into the liquid electrolytes. Another approach is the design of new constructions of anode materials, such as lithiophilic graphene,[23] nickel foam,[24] and polyimide,[25] which have the effect of inhibiting the growth of Li dendrites and reducing the huge volume changes during Li insertion and extraction. It is well known that solid electrolytes have the potential to mechanically block the growth of Li dendrites,[26-28] which has also been predicted by the model of Monroe and Newman.[29] Unfortunately, the most commonly investigated solid electrolyte materials (*e.g.* polymers and ceramics) still have some weaknesses when they are used in practical batteries at room temperature, including insufficient ionic conductivity and high electrode–electrolyte interfacial resistance.[30,31] Some sulfide based and garnet type solid electrolytes have ionic conductivities comparable to those of liquid electrolytes, but the growth of Li dendrite through grain boundaries is still a major problem.[32] Therefore, it is difficult to develop a solid electrolyte that can completely block the growth of Li dendrite; still, the substitution of inflammable organic electrolytes by a flame-resistant one would dramatically enhance the safety of Li batteries.

Ionic liquids (ILs) are liquid-state organic salts with several superior properties: high flame resistance, negligible vapor pressure, good ion conductivity, and excellent electrochemical stability.[33-36] Accordingly, immobilization of ILs within a porous inorganic matrix has been widely considered as a new type of solid-state electrolytes for LBs, which combine both the advantages of inorganic materials (avoiding liquid leakage and sufficient mechanical strength) and ILs (high ionic conductivity at room temperature).[37,38] These quasi-solid-state electrolytes exhibit rather high ion conductivities which are comparable to those of bulk ILs.[39] There have been also some reports of quasi-solid-state electrolytes prepared by the sol–gel polymerization of

[a]*Jiangsu Key Laboratory of Advanced Functional Polymer Design and Application, Department of Polymer Science and Engineering, College of Chemistry, Chemical Engineering and Materials Science, Soochow University, Suzhou 215123, P. R. China. E-mail: liyi@suda.edu.cn*

[b]*College of Mechanical and Energy Engineering, Xiamen Key Lab of Marine Corrosion and Smart Protective Materials, Jimei University, Xiamen 361021, China. E-mail: qihui.wu@jmu.edu.cn; Tel: +86-295-6183523*

Paper

large organic molecules; however, it should be noted that the polymerization reaction would create a large number of volatile by-products such as water, methanol, and format esters, which lead to a relatively long drying period, and cause the environmental pollution, thus strongly affecting the electrochemical properties of the polymer electrolytes.[40,41]

In this article, we report a quasi-solid-state electrolyte composed of helical silica nanofibers (HSNFs) inorganic matrix and [BMI] [TFSI] IL, where [BMI][TFSI] is 1-butyl-3-methylimidazolium bis(trifluoromethyl-sulfonyl)amide. When the gel-like electrolyte is soaked into LiTFSI salt (Li bis(tri-fluoromethanesulfonimide)), it exhibits ionic conductivity similar to those of liquid electrolytes at room-temperature. When the as-obtained electrolyte was tested in a LiFePO₄/Li full cell, the solid-state battery delivers good reversible capacity and superior rate stability.

2. Experimental

2.1 Chemicals

Gelator D-ValPyBr was synthesized according to the literature.[42] LiTFSI and LiFePO₄ was obtained from Aldrich. [BMI][TFSI] was bought from Shanghai Macklin Biochemical Co., Ltd. Tetraethyl orthosilicate (TEOS), ammonia solution (25 wt%) and 1-propanol were purchased from Sinopharm Chemical Reagent Co., Ltd. All the reagents were used without further purification.

2.2 Synthesis of helical silica nanofibers gel electrolyte (HSNGE)

The synthesis process is as follows: 100 mg gelator D-ValPyBr (0.29 mmol) was dissolved in 10.5 mL 1-propanol (with volume ratio of water to 1-propanol as 3 : 7) and 4.5 mL aqueous NH_3 (10.0 wt%) mixture, then 200 mg TEOS (0.95 mmol) was added into the solution drop by drop under a shear flow. After sol–gel polymerization, the mixture turned to transparent solution within 3 min after finishing dropping the TEOS, then the mixture was kept at 0 °C for 1 day and a translucent gel was obtained. After that, the reaction mixture was kept at 80 °C for 4 day under a static condition. Helical silica nanofibers were obtained after removing the template by the calcination performed in a box furnace in air. The as-prepared silica was punched on a microtome with a radius of 8 mm and transferred to the Ar-filled glove box after vacuumed at 70 °C for 24 h. A Li salt–ionic liquid solution (Li–IL) of molality 1 mol L⁻¹ was prepared by adding a proper amount of LiTFSI to the ionic liquid. The as-prepared silica was then transferred to a container filled with IL electrolyte. After sufficiently soaked for more than 1 day, the helical silica nanofibers gel electrolyte was thus obtained and denoted as HSNGE. The production process of HSNGE is indicated in Scheme 1.

2.3 Methods

Field emission scanning electron microscopy (FE-SEM, S-4800, Hitachi) was used to characterize the morphologies and structure of the products with acceleration voltage of 3.0 kV. Transmission electron microscopy (TEM) and high-resolution TEM
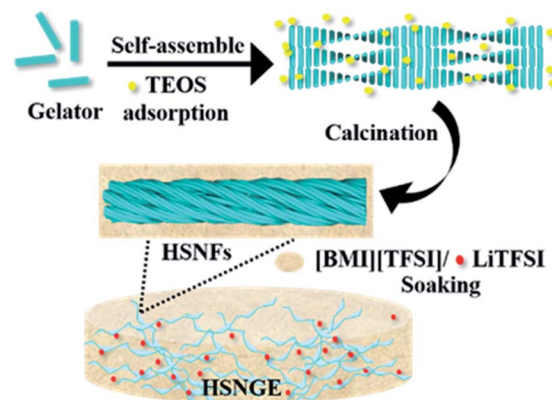
Scheme 1 A quasi-solid-state electrolyte of high-ionic conductivity is constructed from an inorganic matrix composed of helical silica nanofibers (HSNFs) derived from self-assembly of chiral gelators.

(HRTEM) images were collected from a FEI Tecnai G220 system at 200 kV. Thermogravimetric analysis (TGA) was performed on a Thermal Analysis TG/TGA 6300 instrument at a heating rate of 10 °C min⁻¹ under the nitrogen atmosphere. Wide-angle X-ray diffraction (WAXRD) patterns were recorded on an X'Pert-Pro MPD X-ray diffractometer (Cu Kα radiation, λ = 0.154 nm). N_2 sorption isotherms were measured on a Micromeritics Tristar II 3020 instrument. The Brunauer–Emmett–Teller (BET) method was used for the specific surface area, while the Barrett–Joyner–Halon (BJH) method was applied to calculate the pore size distribution from the N_2 adsorption isotherm.

2.4 Electrochemical test

The electrochemical properties of HSNGE electrolyte were evaluated in a LiFePO₄/HSNGE/Li full cell. The cathode was composed of LiFePO₄, acetylene black (AB), and polyvinylidene fluoride (PVDF) binder (dissolved in N-methylpyrrolidone) at a mass ratio of 8 : 1 : 1. The ingredients were mixed to form a slurry, which was then uniformly coated on an Al foil current collector, followed by drying overnight to obtain the cathode. The active material load on the cathode is 1.74 mg cm⁻². A metallic Li foil was used as the counter electrode and HSNGE was used as the electrolyte (and separator). The CR2016 coin-type cells were assembled in an Ar-filled glove box, then charged and discharged at 0.2C within a voltage range from 4.2 to 2.5 V at room temperature. Current rate was estimated using a nominal capacity of 170 mA h g⁻¹ (1C) for the Li/LiFePO₄ cell. Cyclic voltammetry (CV) measurements were performed using an electrochemical workstation (CHI660D, CH Instruments) between 4.2 and 2.5 V at various scan rates. The electrochemical impedance was acquired using an electrochemical workstation (Metrohm Autolab B.V.) in the frequency range of 100 KHz to 10 MHz with an AC amplitude of 10 mV. The ionic conductivity (σ) was determined from impedance spectra. The equation $\sigma = L/R_bS$ was used to calculate the ionic conductivity, where R_b is the resistance of the bulk electrolyte and L is the thickness of electrolyte membrane, and S is the area of the electrode. The Li ion transference number (t_{Li^+}) of the HSNGE at room

temperature was determined using chronoamperometry in combination with impedance spectroscopy measurements. A polarization voltage of 80 mV was applied to the symmetrical Li/HSNSE/Li cell in the chronoamperometry measurement, and the initial current I_0 and the steady-state current I_s were measured. Impedance spectra were acquired before and after polarization to determine the initial and the steady-state bulk resistances, R_b^0 and R_b^s, and interfacial resistances, R_I^0 and R_I^s. Then the following eqn (1) was used to calculate the t_{Li^+}.

$$t_{Li^+} = I_s R_b^0 (\Delta V - I_0 R_I^0)/[I_0 R_b^s (\Delta V - I_s R_I^s)] \tag{1}$$

The electrochemical stability of the HSNSE was examined using a linear sweep voltammetry (LSV) in a 3-electrode configuration where stainless steel was used as working electrode and Li metal as both the counter and reference electrodes. The voltage was swept between 2.0 and 7.0 V (V *vs.* Li/Li$^+$) with a scan rate of 5.0 mV s^{-1}. The charge/discharge cycling tests of the symmetrical Li/HSNGE/Li cells were performed with a Land CT2001A cell tester at room temperature under different current densities with 16 min charge and 16 min discharge time.

3. Results and discussion

Due to the weak intermolecular forces (such as hydrogen bond and van der Waals forces), chiral low-molecular-weight amphiphiles derived from amino acids can self-assemble into various helical nanostructures.[43–45] When the self-assemblies of D-Val-PyBr were used as the templates as mentioned in the experimental section, helical silica nanofibers were obtained after removing the organic template by calcination. In general, the obtained silica is white hard powder; however, we found that if the sol–gel preparation was carried out under dilute D-ValPyBr concentration and high-volume ratio of 1-propanol to water, the

as-obtained silica products are flexible and like sponge or cotton. A pressed pallet of it is shown in Fig. 1a. They can soak up large amount of small organic liquid owing to their mesoporous structure. The FE-SEM and TEM (Fig. 1b and c) observation under different magnifications indicate that the helical nanofibers with lengths of dozens of microns are constructed by bundles of ultrafine tubular nanofibers in a right-handed helix. HR-TEM image (Fig. S1†) reveals that the inner diameters and outer diameter of these helical tubular nanofibers are about 8 nm and 22 nm, respectively. After a sufficient soak in the selected IL, the quasi-solid-state electrolyte film was obtained. The amount of IL electrolyte confined into the HSNFs is calculated from the mass difference of the dried HSNFs film before and after soaking. Almost ten times the mass of the IL electrolyte can be impregnated in the HSNFs. The as-obtained HSNGE film is self-standing, with a thickness of about 0.40 mm, and a gel-like transparent appearance, hinting high Li-IL volume, as depicted in Fig. 1d. It is interesting to note that the opaque silica film became optically transparent after being completely immersed in the IL electrolytes, implying that the spaces and channels between the nanofibers have been completely filled with the liquid to minimize scattering of visible light. The FE-SEM and TEM images (Fig. 1e and f) reveal that the HSNGE has the same nanofiber morphology as that of HSNFs, showing the good stability of the silica structure. WAXRD patterns provide insight into the nature of HSNSE (Fig. S2†), which indicate that the HSNGE contains amorphous silica matrix coexisting with the ionic liquid.[46]

The N$_2$ adsorption–desorption isotherms and the BJH pore size distribution plots calculated from the adsorption branch for the nano-textural structure of HSNFs and HSNGE are shown in Fig. 2. Type-IV isotherms with H3-hysteresis loops at relative pressure (P/P_0) between 0.8 and 1.0 are showed in Fig. 2a, which originates from the voids within and among the nanofibers,
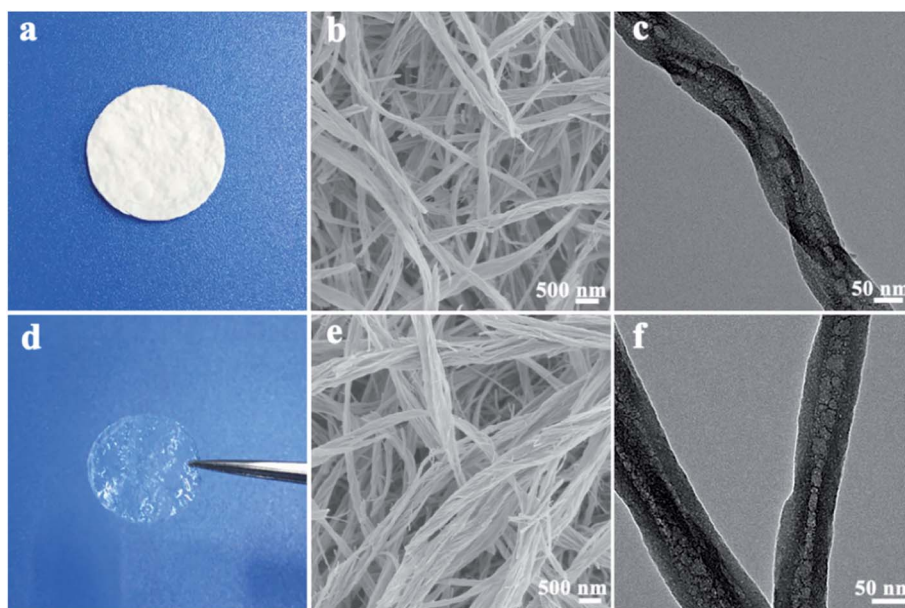

Fig. 1 Photographs (a and d), FE-SEM (b and e) and TEM (c and f) images of the HSNFs (a–c) and the HSNGE (d–f).
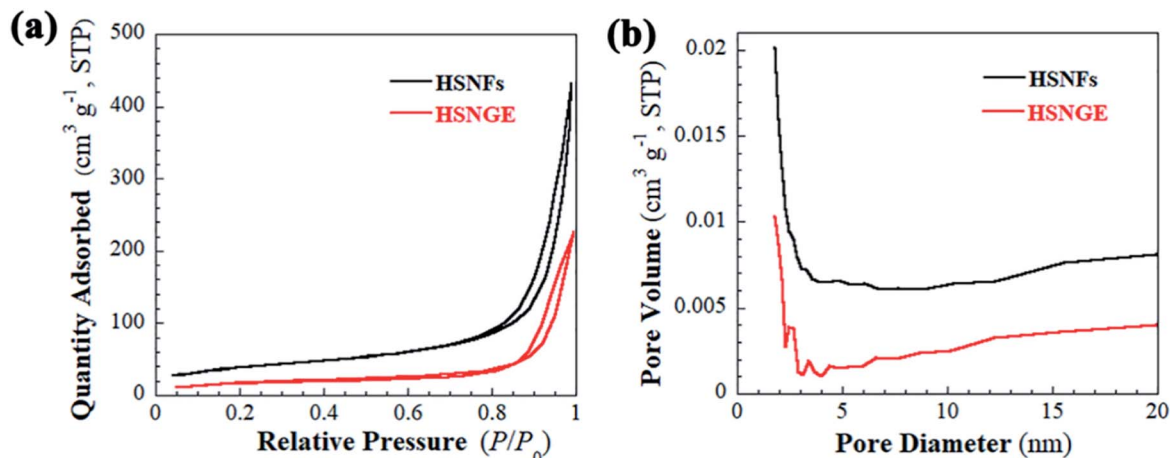
Fig. 2 (a) N$_2$ adsorption−desorption isotherms of HSNFs and HSNGE; (b) BJH pore size distribution plots calculated from the adsorption branch.

indicating the existence of mesopores as well as micropores.[47] The specific surface area and pore volume of HSNFs matrix are 135 m^2 g^{-1} and 0.6 cm^3 g^{-1}, respectively. No sharp peaks are observed and most pores are less than 10 nm in the BJH pore size distribution plot (Fig. 2b). Furthermore, a significant decrease of N$_2$ uptake in the region of P/P_0 above 0.80 clearly is observed upon soaking the helical silica into IL electrolyte, which indicates that the large inter-particle space between neighboring nanofibers is efficiently reduced.[48] It should be noted that, in principle, a large number of mesopores and micropores within the silica nanofibers should have capillary effects to prevent liquid leakage and evaporation.[49] In order to evaluate the thermal stability of HSNGE, TGA analysis was measured in N$_2$ (shown in Fig. S3†). It can be found that the as-obtained HSNGE shows almost the same degraded tendency as the IL, and its decomposition temperature (5% of original weight loss) is about 370 °C, indicating that HSNGE has excellent thermal stability. The remaining about 9% of the weight is the residual helical silica matrix, and thus we can estimate that the weight of the restricted IL electrolyte in HSNGE is almost 10 times the weight of the HSNFs matrix. For 12 mg HSNFs matrix, the loading amount of IL electrolytes is about 120 mg, implying that the synthesized silica has a high adsorption capacity to IL.

Ionic conductivity (σ) of the solid-state electrolyte was determined at different temperatures, as presented in Fig. 3a. As expected, the σ increases (and the bulk resistance of electrolyte decreases, see Fig. S4†) exponentially with increasing temperature; the activation energy for ionic conduction is 0.36 eV, as estimated from the slope of ln(σT) against $1/T$, which is 34.6 kJ mol^{-1}.[50] The conductivity of the HSNGE obtained in this work is calculated to be 3.0 mS cm^{-1} at 25 °C, which is on the same order of magnitude as that of the pristine ILs. The conductivity is sufficient for a normal LBs operation (1 mS cm^{-1} at ambient temperature).[51]

The electrochemical stability of electrolytes over the operating voltage range of LBs is also an important requirement for the practical cell operation. When the battery is running, a suitable electrolyte must be chemically stable against the

electrode materials within the operating potential window. The operating voltage of commercial LBs usually is 4.2 V (*vs.* Li/Li$^+$), while for high-voltage LBs even reaches 4.8 V (*vs.* Li/Li$^+$). Therefore, the LSV measurements was performed between 2.0 and 7.0 V (V *vs.* Li/Li$^+$) at a scanning rate of 5.0 mV s^{-1} with stainless steel as the working electrode and Li metal as both the reference electrode and counter electrode. As shown in Fig. 3b, it is seen that no significant oxidation was observed below 5.6 V, demonstrating that fabricated HSNGE has good electrochemical stability, which can be attributed to the inorganic silica backbone. The Li-ion transference number (t_{Li^+}) of the HSNGE was determined by the Bruce–Vincent equation with a symmetric Li|HSNGE|Li cell with a constant polarization potential of 80 mV at room temperature. The chronoamperometry profile of the HSNGE is shown in Fig. 3c, the variation of current with time in the polarization process shows that the current density reached a steady value of 0.09 mA cm^{-2} from the initial state of 0.37 mA cm^{-2} before polarization. The Nyquist impedance spectra of the cell under initial and steady-state current conditions are shown in Fig. 3d, indicating that the interfacial resistance increased from 75 to 86 Ohm cm^{-2} due to the change at the interphase conditions during concentration polarization. The calculated t_{Li}^+ for the HSNGE value is 0.16, suggesting that the majority of the ionic conductive species in IL are [BMI]$^+$ and [TFSI]$^-$ rather than Li$^+$.[52] These results reveal that the as-prepared HSNGE are promising electrolyte candidate for LBs.

Symmetrical Li|HSNGE|Li cells were also fabricated for evaluating the interfacial stability of HSNGE with Li metal electrode and its mechanical stability against Li dendrites growth in a galvanostatic cycling experiment, which was periodically charged and discharged at a constant current density to mimic the Li stripping and plating process at room temperature. The time-dependent voltage curves during cycling tests are depicted in Fig. 4; the stable voltage can be obtained, which indicates that a stable interface is formed.[53] As expected, the voltage profile of the symmetric cell is relatively stable during the continuous cycling at 0.05 mA cm^{-2}, indicating a good
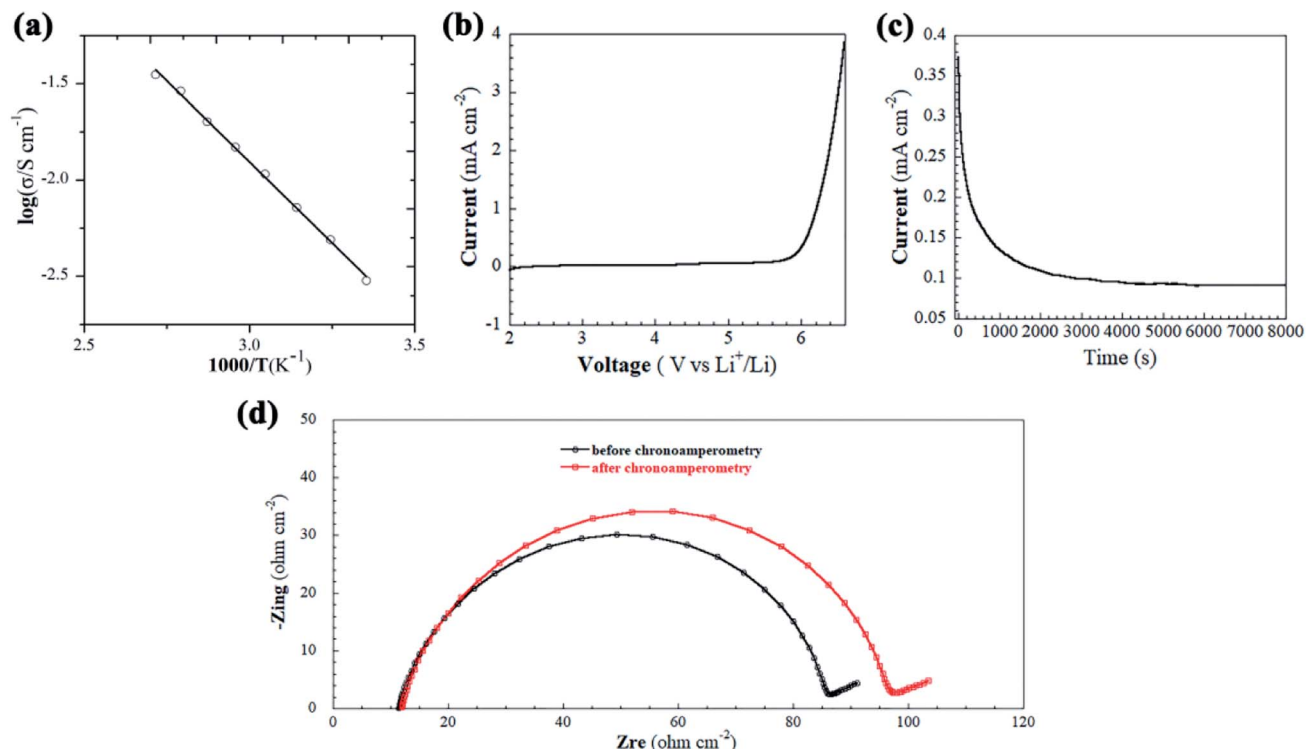
Fig. 3 (a) Ionic conductivity of HSNGE measured at different temperatures, the fitting straight line is log $\sigma = -1.68 \times 1000/T + 3.15$; (b) LSV of HSNGE; (c) current–time profile of the symmetrical Li|HSNGE|Li cell during polarization at an applied voltage of 80 mV at room temperature; (d) Nyquist impedance spectra of the cell under initial and steady-state current conditions.

compatibility between HSNGE and Li metal electrode. It is likely that stable SEI films were formed on the Li metal.[54] There was no cell failure caused by a short circuit due to dendrite growth when the current density was increased to 0.1 mA cm^{-2}. The

electrochemical stability of the cell would be further supported by the stable cycling up to 200 cycles at a high current density (2C).
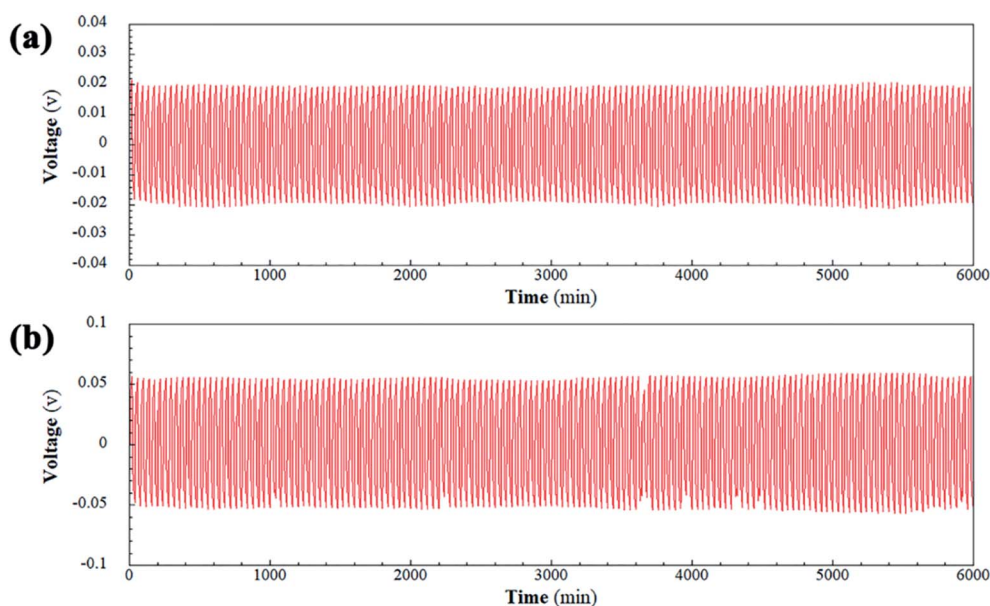

Fig. 4 Voltage profiles for Li plating/striping experiment as a function of time for Li|HSNGE|Li symmetric lithium coin cell cycled at the current density of (a) 0.05 mA cm^{-2} and (b) 0.1 mA cm^{-2}.

To demonstrate the feasibility of the HSNGE in the LBs, quasi-solid-state LiFePO$_4$|HSNGE|Li cell was assembled and evaluated *via* cycling in a voltage range of 4.2 and 2.5 V at room temperature. The CV curves are depicted in Fig. 5a. The redox peaks gradually expand but remain sharp when the scan rate increases from 0.1 to 0.5 mV s^{-1}. These sharp redox peaks indicate that the unique battery configuration of the LiFePO$_4$ cathode. Highly conductive HSNGE can maintain high stability of the cathode and electrolyte interface, and also maintain the electrochemical stability at different scan rates. The charge–discharge voltage profiles of the LiFePO$_4$|HSNGE|Li cell are shown in Fig. 5b by cycling at a constant charge/discharge current density of 0.1C. The battery delivers an initial charge and discharge capacity of 156.4.0 and 138.3 mA h g^{-1} with an 88.4% coulombic efficiency in first cycle due to low interfacial side reactions compared to the liquid electrolyte. The irreversible capacity loss at the first cycle is mainly due to the formation of the protective SEI films on the surface of Li anode.[55] The rate performance of the cell at various current densities from 0.1 to 2C at room temperature is illustrated in Fig. 5c. The battery is capable of continuous cycling at each current rate and provides a stable discharge capacity. The reversible capacities are 126, 102, 67, 43, 19 mA h g^{-1} at rates 0.1, 0.2, 0.5, 1 and 2C, respectively. Obviously, the discharge plateau voltage decreases with the increase of the current rate (see Fig. S5†), which is attributed to the enhancement of battery polarization.[56] In addition, note that when the rate goes back to 0.1C, the discharge capacity can recover its original discharge capacities, which indicates that LiFePO$_4$|HSNGE|Li cell possesses excellent rating capability. In order to detect the cell stability at high rate, the cycling performance of the cell is also preliminarily

examined as displayed in Fig. 5d, a discharge capacity of 118.1 mA h g^{-1} at 0.1C can be gained after 200 cycles with coulombic efficiency of 99.7%. The photograph of HSNGE after cycling was taken. As seen in Fig. S6a,† the solid-state electrolyte can still remain self-standing pellet. Fig. S6b† shows that the helical nanofibers in HSNGE still maintain the initial constructive, suggesting excellent structural stability.

Electrochemical impedance spectroscopy (EIS) measurement was performed to study the interphase reactions of the cell (Fig. S7†). An interfacial polarization resistance of 55.5 Ohm cm^{-2} before cycling and 33.5 Ohm cm^{-2} after 50 cycles can be seen from the Nyquist plots, which can be attributed to some conditioning of the HSNGE/electrode and Li/electrolyte interfaces during cycling.[50] The equivalent circuit also provided as inset in Fig. S7,† in which R_b is the bulk resistance of electrolyte (intercept with the real axis at high frequencies) and R_{ct} is charge transfer resistance, CPE is the electrical double layer capacitor corresponding to the half circle and Z_w is Warburg resistance. Zhang *et al.* prepared solid electrolytes with liquid-like room-temperature ionic conductivity (2.5 mS cm^{-1}) by taking advantage of the unique nanoarchitecture of hollow silica spheres to confine that IL in hollow space could afford high conductivities.[57] Ito *et al.* reported lithium-ion-conducting solid electrolyte material comprising silica nanoparticles and IL, and the ion conductivity of the solid electrolyte at 75 vol% of Li–IL volume ratio was 0.32–4.4 mS cm^{-1} at 287–348 K.[38] However, it should be pointed out that nanoparticles or spheres are prone to phase separation and agglomeration,[58] which would result in poor cycling performance. Therefore, the long-term stability of solid electrolyte prepared directly from nanoparticles needs to be further improved and discussed. The
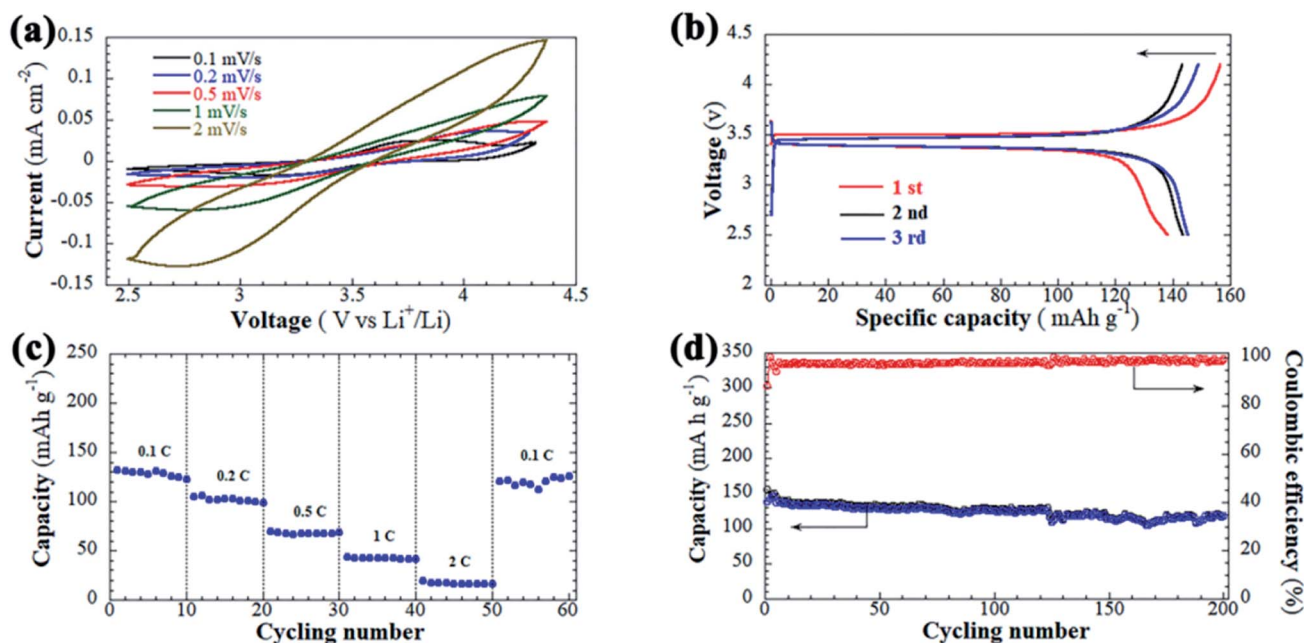

Fig. 5 (a) CV curves of the LiFePO$_4$|HSNGE|Li cell between 4.2 and 2.5 V at various scan rates; (b) potential–capacity profiles at 1st, 2nd, 3rd cycles with 0.1C charge and discharge rate at room temperature; (c) galvanostatic charge capacity at various current densities from 0.1C to 2C; (d) cycling performance of the LiFePO$_4$|HSNGE|Li cell at 0.1C.

application of HSNFs as the inorganic matrix for solid-state electrolyte exhibited rather high chemical, structural, and electrochemical stability when used in LBs. The electrochemical results imply that the HSNGE electrolyte is a promising quasi-solid-state electrolyte for practical safer LBs.

4. Conclusions

We have designed and synthesized a quasi-solid-state electrolyte composed of ionic liquid electrolytes impregnated in helical silica nanofibers. This electrolyte exhibited good thermal stability (up to ~370 °C), wide electrochemical window, and desirable room-temperature ionic conductivity (3.0 mS cm^{-1}). In particular, it exhibited good compatibility with active Li metal anode. When the electrolyte is used to construct a Li/LiFePO$_4$ cell, satisfactory rate capability and acceptable cycling performance were demonstrated, implying that the HSNGE is a promising candidate for safer Li batteries. Furthermore, the strategy developed here for the electrolyte based on a helical silica nanofibers matrix is applicable to other kinds of solid-like electrolytes though changing the ion species in the ionic liquid, offering an effective approach to the development of promising electrolytes for safer all-solid-state Li batteries.

Conflicts of interest

There are no conflicts to declare.

Acknowledgements

References

1 K. Kang, Y. S. Meng, J. Bréger, C. P. Grey and G. Ceder, Electrodes with high power and high capacity for rechargeable lithium batteries, *Science*, 2006, **311**, 977–980.

2 B. Kang and G. Ceder, Battery materials for ultrafast charging and discharging, *Nature*, 2009, **458**, 190–193.

3 J. M. Tarascon and M. Armand, Issues and challenges facing re-chargeable lithium batteries, *Nature*, 2001, **414**, 359–367.

4 B. Scrosati and J. Garche, Lithium batteries: status, prospects and future, *J. Power Sources*, 2010, **195**, 2419–2430.

5 N. S. Choi, Z. Chen, S. A. Freunberger, X. Ji, Y. K. Sun, K. Amine, G. Yushin, L. F. Nazar, J. Cho and P. G. Bruce, Challenges facing lithium batteries and electrical double-layer capacitors, *Angew. Chem., Int. Ed.*, 2012, **51**, 9994–10024.

6 C. X. Zu and H. Li, Thermodynamic analysis on energy densities of batteries, *Energy Environ. Sci.*, 2011, **4**, 2614–2624.

7 D. Aurbach and Y. Cohen, The application of atomic force microscopy for the study of Li deposition processes, *J. Electrochem. Soc.*, 1996, **143**, 3525–3532.

8 W. Xu, J. Wang, F. Ding, X. Chen, E. Nasybulin, Y. Zhang and J. G. Zhang, Lithium metal anodes for rechargeable batteries, *Energy Environ. Sci.*, 2014, **7**, 513–537.

9 C. P. Yang, Y. X. Yin, S. F. Zhang, N. W. Li and Y. G. Guo, Accommodating lithium into 3D current collectors with a submicron skeleton towards long-life lithium metal anodes, *Nat. Commun.*, 2015, **6**, 8058.

10 R. Selim and P. Bro, Some observations on rechargeable lithium electrodes in a propylene carbonate electrolyte, *J. Electrochem. Soc.*, 1974, **121**, 1457–1459.

11 R. D. Rauh and S. B. Brumme, Effect of additives on lithium cycling in propylene carbonate, *Electrochim. Acta*, 1977, **22**, 75–83.

12 D. Aurbach, E. Zinigrad, Y. Cohen and H. Teller, A short review of failure mechanisms of lithium metal and lithiated graphite anodes in liquid electrolyte solutions, *Solid State Ionics*, 2002, **148**, 405–416.

13 J. B. Goodenough and Y. Kim, Challenges for rechargeable Li batteries, *Chem. Mater.*, 2010, **22**, 587–603.

14 Y. Lu, Z. Tu and L. A. Archer, Stable lithium electrodeposition in liquid and nanoporous solid electrolytes, *Nat. Mater.*, 2014, **13**, 961–969.

15 Y. Liu, Q. Liu, L. Xin, Y. Liu, F. Yang, E. A. Stach and J. Xie, Making Li-metal electrodes rechargeable by controlling the dendrite growth direction, *Nat. Energy*, 2017, **2**, 17083.

16 Y. Lu, S. K. Das, S. S. Moganty and L. A. Archer, Ionic liquid-nanoparticle hybrid electrolytes and their application in secondary lithium-metal batteries, *Adv. Mater.*, 2012, **24**, 4430–4435.

17 F. Ding, W. Xu, G. L. Graff, J. Zhang, M. L. Sushko, X. Chen, Y. Shao, M. H. Engelhard, Z. Nie, J. Xiao, X. Liu, P. V. Sushko, J. Liu and J. G. Zhang, Dendrite-free lithium deposition via self-healing electrostatic shield mechanism, *J. Am. Chem. Soc.*, 2013, **135**, 4450–4456.

18 W. Li, H. Yao, K. Yan, G. Zheng, Z. Liang, Y. M. Chiang and Y. Cui, The synergetic effect of lithium polysulfide and lithium nitrate to prevent lithium dendrite growth, *Nat. Commun.*, 2015, **6**, 7436–7443.

19 S. Choudhury and L. A. Archer, Lithium fluoride additives for stable cycling of lithium batteries at high current densities, *Adv. Electron. Mater.*, 2016, **2**, 1500246.

20 S. K. Jeong, H. Y. Seo, D. H. Kim, H. K. Han, J. G. Kim, Y. B. Lee, Y. Iriyama, T. Abe and Z. Ogumi, Suppression of dendritic lithium formation by using concentrated electrolyte solutions, *Electrochem. Commun.*, 2008, **10**, 635–638.

21 J. Qian, W. A. Henderson, W. Xu, P. Bhattacharya, M. Engelhard, O. Borodin and J. G. Zhang, High rate and stable cycling of lithium metal anode, *Nat. Commun.*, 2015, **6**, 6362.

22 R. Miao, J. Yang, X. Feng, H. Jia, J. Wang and Y. Nuli, Novel dual-salts electrolyte solution for dendrite-free lithium-metal based rechargeable batteries with high cycle reversibility, *J. Power Sources*, 2014, **271**, 291–297.

23 D. Lin, Y. Liu, Z. Liang, H. W. Lee, J. Sun, H. Wang, K. Yan, J. Xie and Y. Cui, Layered reduced graphene oxide with

nanoscale interlayer gaps as a stable host for lithium metal anodes, *Nat. Nanotechnol.*, 2016, **11**, 626–632.

24 S. S. Chi, Y. Liu, W. L. Song, L. Z. Fan and Q. Zhang, Prestoring lithium into stable 3D nickel foam host as dendrite-free lithium metal anode, *Adv. Funct. Mater.*, 2017, **27**, 1700348.

25 Y. Liu, D. Lin, Z. Liang, J. Zhao, K. Yan and Y. Cui, Lithium-coated polymeric matrix as a minimum volume-change and dendrite-free lithium metal anode, *Nat. Commun.*, 2016, **7**, 10992.

26 R. Khurana, J. L. Schaefer, L. A. Archer and G. W. Coates, Suppression of lithium dendrite growth using cross-linked polyethylene/poly (ethylene oxide) electrolytes: a new approach for practical lithium-metal polymer batteries, *J. Am. Chem. Soc.*, 2014, **136**, 7395–7402.

27 S. Srivastava, J. L. Schaefer, Z. Yang, Z. Tu and L. A. Archer, Polymer-particle composites: phase stability and applications in electrochemical energy storage, *Adv. Mater.*, 2014, **26**, 201–234.

28 V. Thangadurai, S. Narayanan and D. Pinzaru, Garnet-type solid-state fast Li ion conductors for Li batteries: critical review, *Chem. Soc. Rev.*, 2014, **43**, 4714–4727.

29 C. Monroe and J. Newman, The impact of elastic deformation on deposition kinetics at lithium/polymer interfaces, *J. Electrochem. Soc.*, 2005, **152**, A396–A404.

30 Z. Gadjourova, Y. G. Andreev, D. P. Tunstall and P. G. Bruce, Ionic conductivity in crystalline polymer electrolytes, *Nature*, 2001, **412**, 520–523.

31 D. Saito, Y. Ito, K. Hanai, T. Kobayashi, N. Imanishi, A. Hirano, Y. Takeda and O. Yamamoto, Carbon anode for dry-polymer electrolyte lithium batteries, *J. Power Sources*, 2010, **195**, 6172–6176.

32 Y. Ren, Y. Shen, Y. Lin and C. W. Nan, Direct observation of lithium dendrites inside garnet-type lithium-ion solid electrolyte, *Electrochem. Commun.*, 2015, **57**, 27–30.

33 B. Garcia, S. Lavallée, G. Perron, C. Michot and M. Armand, Room temperature molten salts as lithium battery electrolyte, *Electrochim.Acta*, 2004, **49**, 4583–4588.

34 H. Sakaebe, H. Matsumoto and K. Tatsumi, Discharge-charge properties of Li/LiCoO$_2$ cell using room temperature ionic liquids (RTILs) based on quaternary ammonium cation - Effect of the structure, *J. Power Sources*, 2005, **146**, 693–697.

35 M. Mansuer, L. Miao, D. Zhu, H. Duan, Y. Lv, L. Li, M. Liu and L. Gan, Facile construction of highly redox active carbons with regular micropores and rod-like morphology towards high-energy supercapacitors, *Mater. Chem. Front.*, 2021, **5**(7), 3061–3072.

36 Z. Zhou, L. Miao, H. Duan, Z. Wang, Y. Lv, W. Xiong, D. Zhu, L. Li, M. Liu and L. Gan, Highly active N, O-doped hierarchical porous carbons for high-energy supercapacitors, *Chin. Chem. Lett.*, 2020, **31**, 1226–1230.

37 P. Barpanda, J. N. Chotard, C. Delacourt, M. Reynaud, Y. Filinchuk, M. Armand, M. Deschamps and J. M. Tarascon, LiZnSO$_4$ made in an ionic liquid: a ceramic electrolyte composite for solid-state lithium batteries, *Angew. Chem., Int. Ed.*, 2011, **50**, 2526–2531.

38 S. Ito, A. Unemoto, H. Ogawa, T. Tomai and I. Honma, Application of quasi-solid-state silica nanoparticle-ionic liquid composite electrolytes to all-solid-state lithium secondary battery, *J. Power Sources*, 2012, **208**, 271–275.

39 M. Mezger, H. Schröder, H. Reichert, S. Schramm, J. S. Okasinski, S. Schöder, V. Honkimäki, M. Deutsch, B. M. Ocko, J. Ralston, M. Rohwerder, M. Stratmann and H. Dosch, Molecular layering of fluorinated ionic liquids at a charged sapphire (0001) surface, *Science*, 2008, **322**, 424–428.

40 M. A. Neouze, J. Le Bideau, F. Leroux and A. Vioux, A route to heat resistant solid membranes with performances of liquid electrolytes, *Chem. Commun.*, 2005, 1082–1084.

41 A. I. Horowitz and M. J. Panzer, High-performance, mechanically compliant silica-based ionogels for electrical energy storage applications, *J. Mater. Chem.*, 2012, **22**, 16534–16539.

42 Y. Yang, M. Suzuki, S. Owa, H. Shirai and K. Hanabusa, Control of mesoporous silica nanostructures and pore-architectures using a thickener and gelator, *J. Am. Chem. Soc.*, 2007, **129**, 581–587.

43 X. Wu, S. Ji, Y. Li, B. Li, X. Zhu, K. Hanabusa and Y. Yang, Helical transfer through nonlocal interactions, *J. Am. Chem. Soc.*, 2009, **131**, 5986–5993.

44 X. Zhang, X. Chu, L. Wang, H. Wang, G. Liang, J. Zhang, J. Long and Z. Yang, Rational design of a tetrameric protein to enhance interactions between self-assembled fibers gives molecular hydrogels, *Angew. Chem., Int. Ed.*, 2012, **51**, 4388–4392.

45 Y. Fu, B. Li, Z. Huang, Y. Li and Y. Yang, Terminal is important for the helicity of the self-assemblies of dipeptides derived from alanine, *Langmuir*, 2013, **29**, 6013–6017.

46 Y. Liu, M. Wang, Z. Li, H. Liu, P. He and J. Li, Preparation of porous aminopropylsilsesquioxane by a nonhydrolytic sol-gel method in ionic liquid solvent, *Langmuir*, 2005, **21**, 1618–1622.

47 H. Sun, Q. Wang, H. Geng, B. Li, Y. Li, Q. H. Wu, J. Fan and Y. Yang, Fabrication of chiral mesoporous carbonaceous nanofibers and their electrochemical energy storage, *Electrochim. Acta*, 2016, **213**, 752–760.

48 X. Li, X. Liu, Y. Ma, M. Li, J. Zhao, H. Xin, L. Zhang, Y. Yang, C. Li and Q. Yang, Engineering the formation of secondary building blocks within the hollow interiors, *Adv. Mater.*, 2012, **24**, 1424–1428.

49 M. Fichtner, Nanoconfinement effects in energy storage materials, *Phys. Chem. Chem. Phys.*, 2011, **13**, 21186–21195.

50 F. Wu, G. Tan, R. Chen, L. Li, J. Xiang and Y. Zheng, Novel solid-state Li/LiFePO$_4$ battery configuration with a ternary nanocomposite electrolyte for practical applications, *Adv. Mater.*, 2011, **23**, 5081–5085.

51 B. M. Wiers, M. L. Foo, N. P. Balsara and J. R. Long, A solid lithium electrolyte via addition of lithium isopropoxide to a metal-organic framework with open metal sites, *J. Am. Chem. Soc.*, 2011, **133**, 14522–14525.

52 Z. Wang, R. Tan, H. Wang, L. Yang, J. Hu, H. Chen and F. Pan, A metal-organic-framework-based electrolyte with

nanowetted interfaces for high-energy-density solid-state lithium battery, *Adv. Mater.*, 2018, **30**, 1704436.

53 Q. Pan, D. M. Smith, H. Qi, S. Wang and C. Y. Li, Hybrid electrolytes with controlled network structures for lithium metal batteries, *Adv. Mater.*, 2015, **27**, 5995–6001.

54 Y. Lu, K. Korf, Y. Kambe, Z. Tu and L. A. Archer, Ionic liquid-nanoparticle hybrid electrolytes: applications in lithium metal batteries, *Angew. Chem., Int. Ed.*, 2014, **53**, 488–492.

55 X. Li, Z. Zhang, S. Li, K. Yang and L. Yang, Polymeric ionic liquid-ionic plastic crystal all-solid-state electrolytes for wide operating temperature range lithium metal batteries, *J. Mater. Chem. A*, 2017, **5**, 21362–21369.

56 S. H. Kim, K. H. Choi, S. J. Cho, E. H. Kil and S. Y. Lee, Mechanically compliant and lithium dendrite growth-suppressing composite polymer electrolytes for flexible lithium-ion batteries, *J. Mater. Chem. A*, 2013, **1**, 4949–4955.

57 J. Zhang, Y. Bai, X. G. Sun, Y. Li, B. Guo, J. Chen, G. M. Veith, D. K. Hensley, M. P. Paranthaman, J. B. Goodenough and S. Dai, Superior conductive solid-like electrolytes: nanoconfining liquids within the hollow structure, *Nano Lett.*, 2015, **15**, 3398–3402.

58 S. Shimano, H. Zhou and I. Honma, Preparation of nanohybrid solid-state electrolytes with liquidlike mobilities by solidifying ionic liquids with silica particles, *Chem. Mater.*, 2007, **19**, 5216–5221.